Supplementary information for Publication

to

Interface-Dependent Ion Migration/Accumulation Controls Hysteresis in $MAPbI_3$ Solar Cells

Igal Levine[1], Pabitra K. Nayak[2], Jacob Tse-Wei Wang[2], Nobuya Sakai[2], Stephan Van Reenen[2], Thomas M. Brenner[1], Sabyasachi Mukhopadhyay[1], Henry J. Snaith,[2], Gary Hodes[1*] David Cahen[1]

[1]Dept. of Materials & Interfaces, Weizmann Inst. of Science, Rehovot, Israel, 76100

[2]Clarendon Laboratory, Dept. of Physics, Univ. of Oxford, Oxford, UK, OX1 3PU

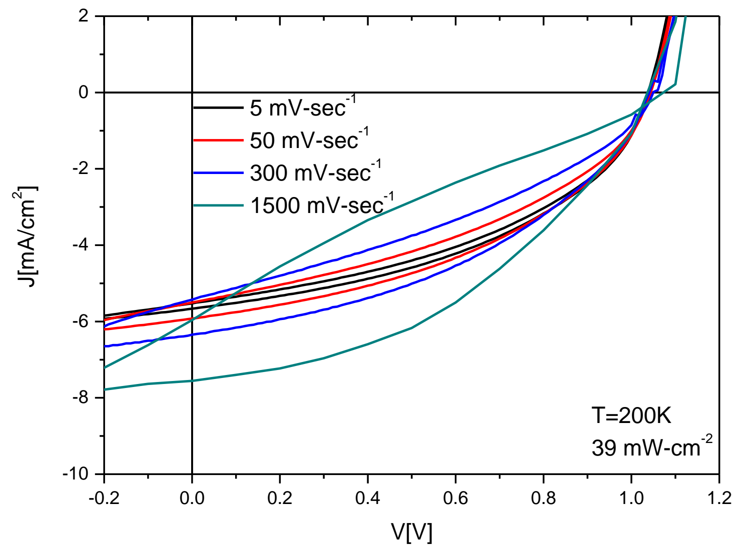

Figure S1: J-V curves measured for the p-i-n cell under 39 mW cm^{-2} light intensity at different scan rates at 200K

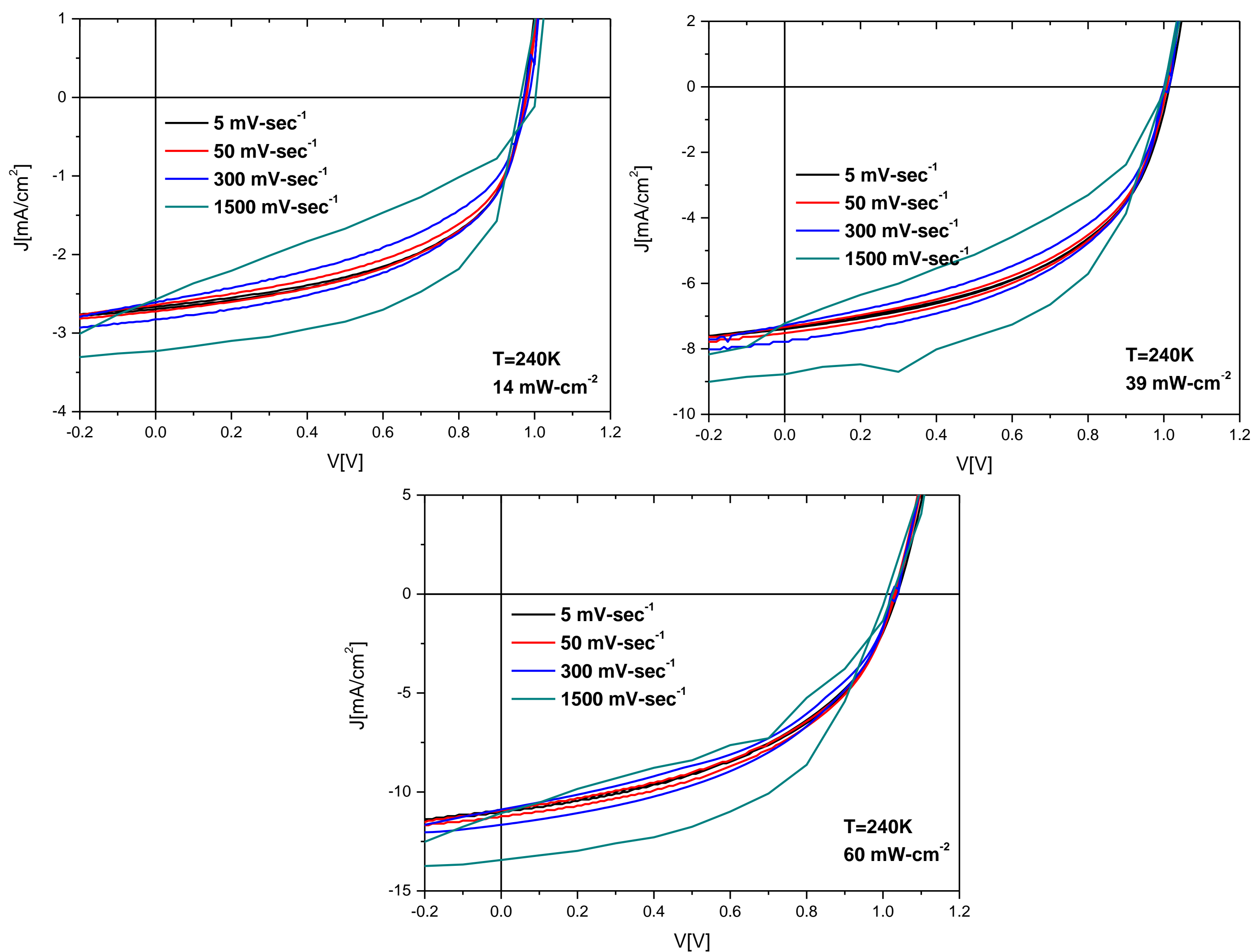

Figure S2: J-V curves for the p-i-n cell measured at 240K under 14 mW cm^{-2} (top left), 39 mW cm^{-2} (top right) and 60 mW cm^{-2} (bottom)

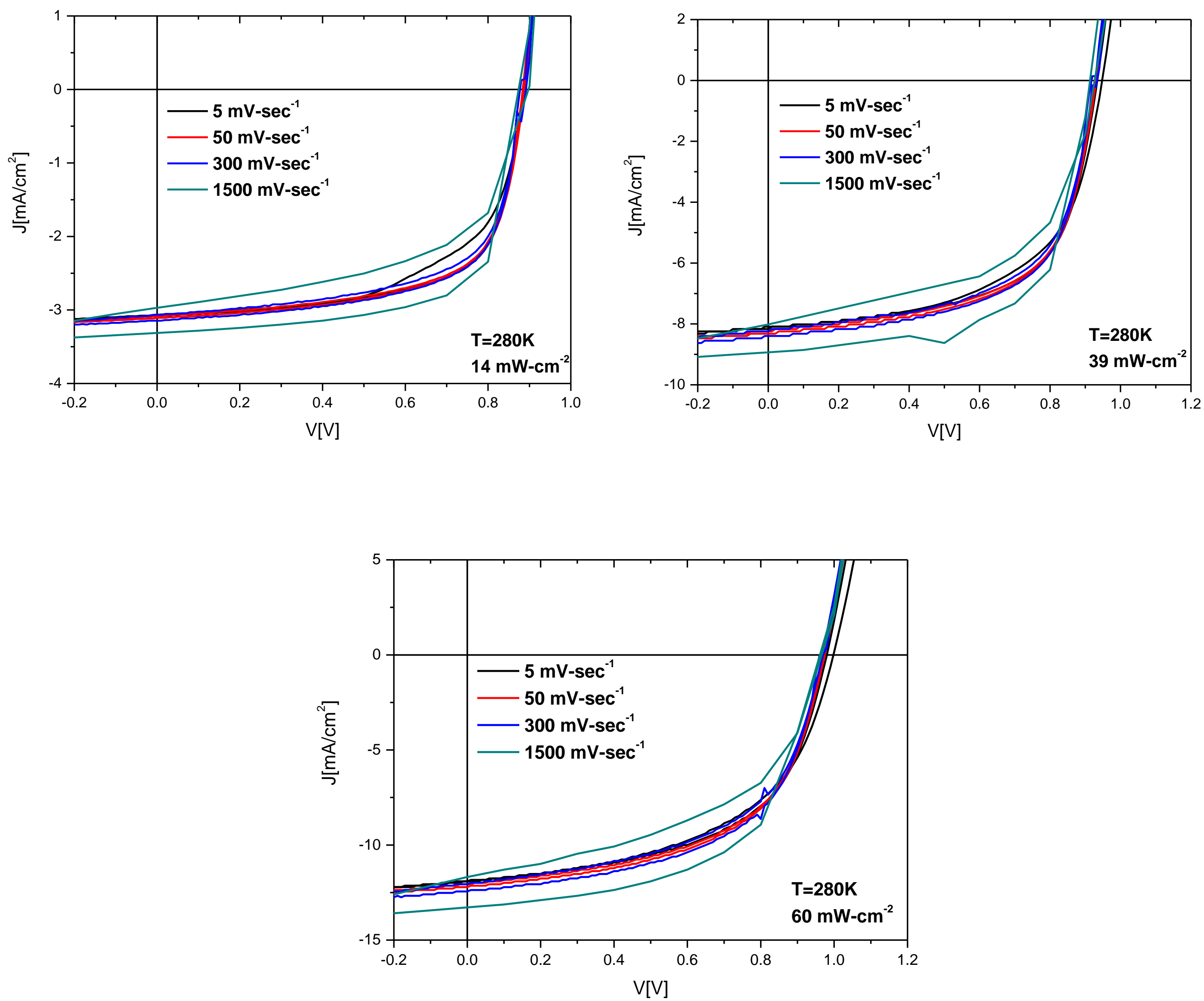

Figure S3: J-V curves for the p-i-n cell measured at 280K under 14 mW cm^{-2} (top left), 39 mW cm^{-2} (top right) and 60 mW cm^{-2} (bottom)

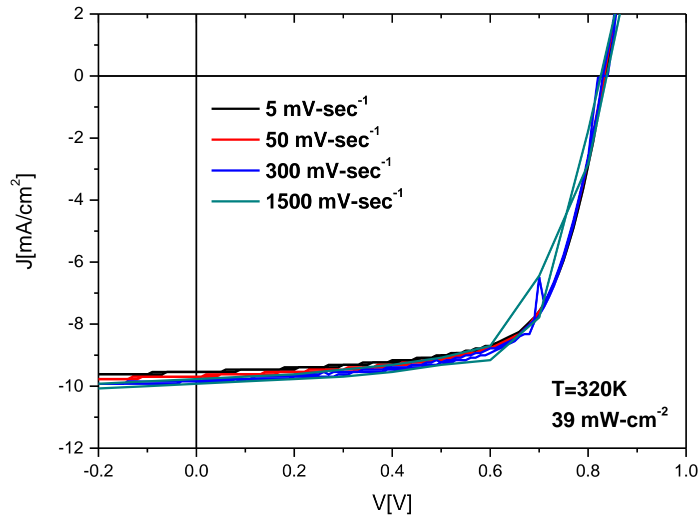

Figure S4: J-V curves for the p-i-n cell measured under 39 mW cm^{-2} light intensity at different scan rates at 320K

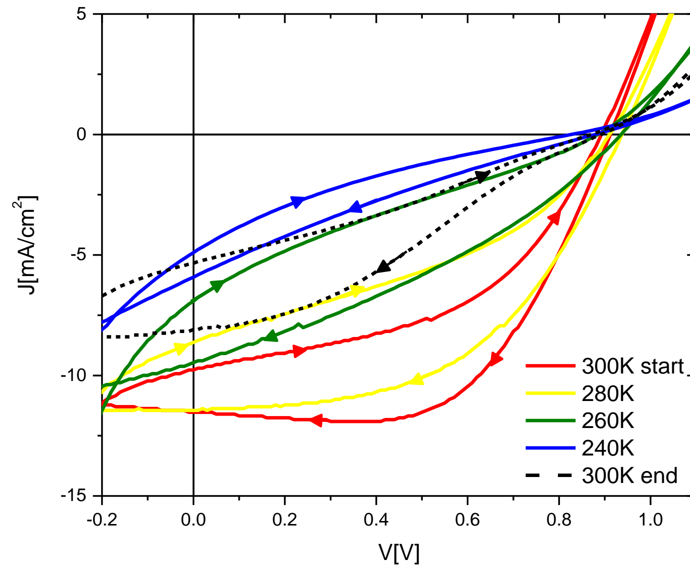

Figure S5: J-V curves of n-i-p device, measured under light intensity of 60 mW cm^{-2} at a scan rate of 50 mV sec^{-1}. The dashed line represents the J-V curve taken after heating back up to 300K; arrows indicate the scan directions.

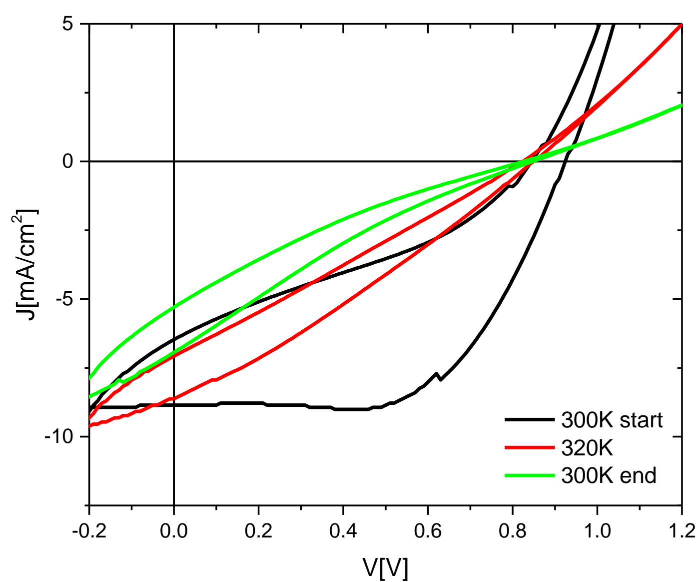

Figure S6: J-V curves of n-i-p device measured under light intensity of 60 mW cm^{-2} at a scan rate of 50 mV sec^{-1} under vacuum.

We note that although the peak in the photocurrent, seen on the J-V curves scanned at 300K on Figures S5&S6 is out of the scope of our work, such a phenomenon was also observed in a recent work done by Sarker et. al[1], in which the absorber was N719 dye.

[1] Sarker, S., Seo, H. W., Jin, Y.-K., Lee, K.-S., Lee, M., & Kim, D. M. (2015). On the Hysteresis of Current Density-Voltage Curves of Dye-sensitized Solar Cells. *Electrochimica Acta*, *182*, 493–499. doi:10.1016/j.electacta.2015.09.083

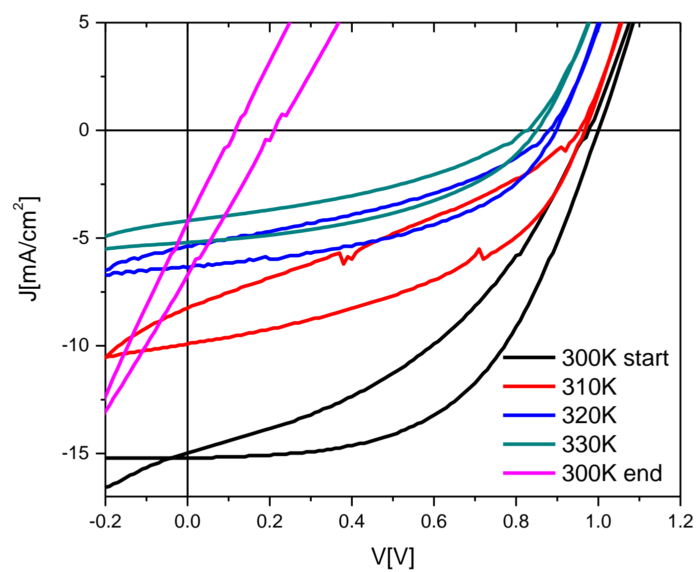

Figure S7: J-V curves of n-i-p device, which underwent heating under ambient conditions, measured under light intensity of 60 mW cm^{-2} at a scan rate of 50 mV sec^{-1}

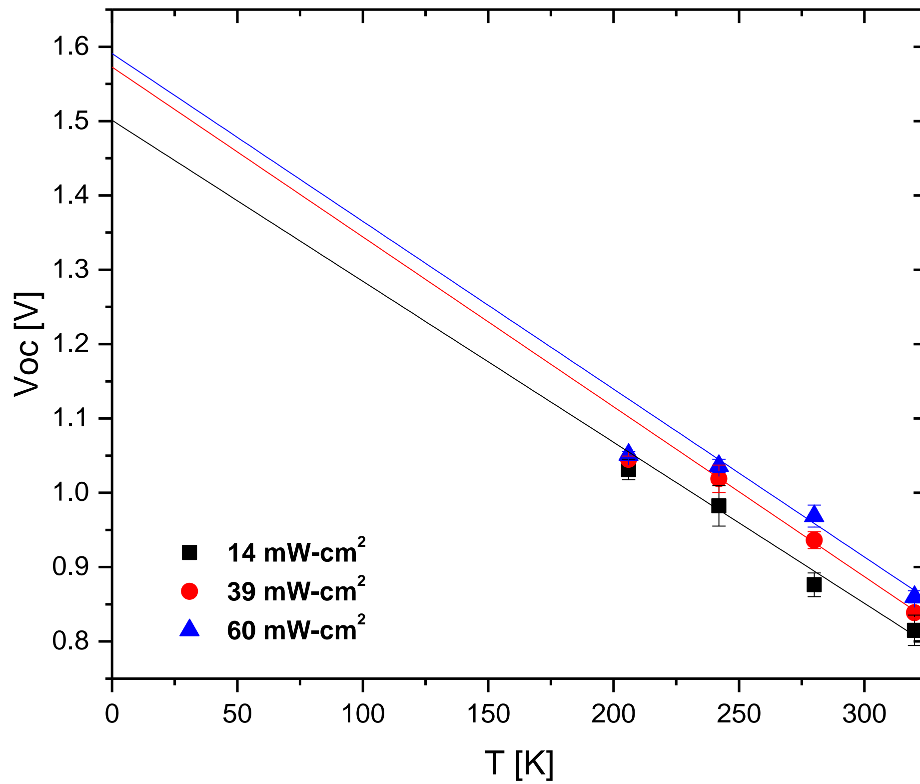

Fig. S8: Voc as a function of temperature for the p-i-n device at the 3 different light intensities that were used to extract the HF values. The values in each temperature are an average of the forward and reverse scans (for the four different scan rates). The error bars denote the standard deviation of the different values.

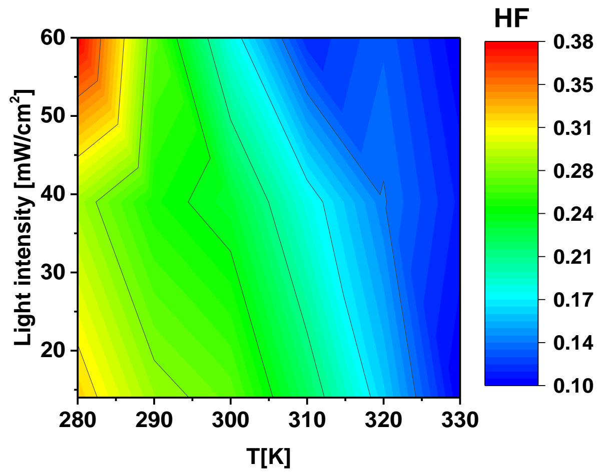
HF
0.38
0.35
0.31
0.28
0.24
0.21
0.17
0.14
0.10
60
50
40
30
20
Light intensity [mW/cm^2]
280
290
300
310
320
330
T[K]

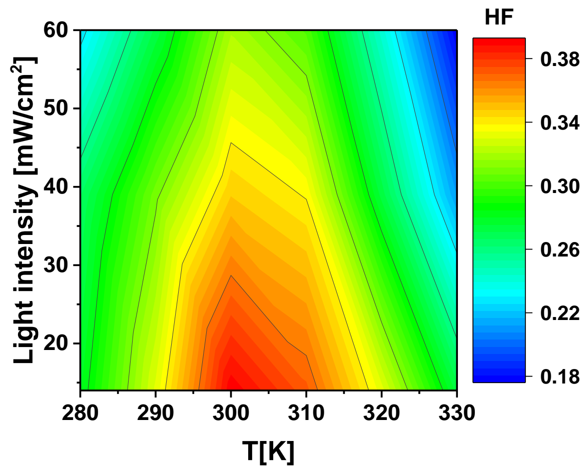
HF
0.38
0.34
0.30
0.26
0.22
0.18
60
50
40
30
20
Light intensity [mW/cm^2]
280
290
300
310
320
330
T[K]

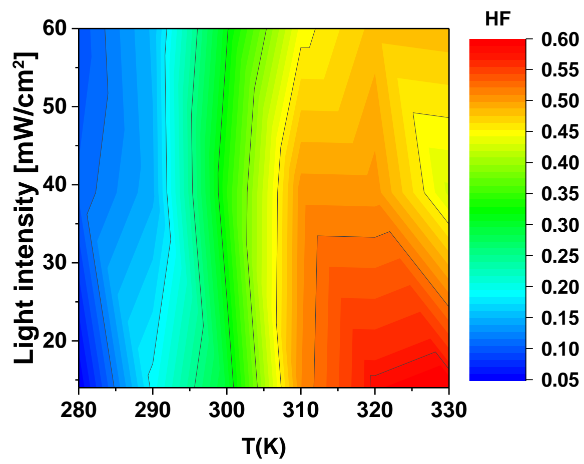
HF
0.60
0.55
0.50
0.45
0.40
0.35
0.30
0.25
0.20
0.15
0.10
0.05
60
50
40
30
20
Light intensity [mW/cm^2]
280
290
300
310
320
330
T(K)

Fig. S9: Hysteresis factor for n-i-p devices as a function of light intensity and temperature for scan rates of 50 (a) 300 (b) and 1500 mV s^{-1} (c). The color map indicates the value of the hysteresis factor ***with a separate scale for each of the scan rate****. While this prevents direct comparison between the different scan rates (which is possible for the figure in the main text) it provides more detail for each scan rate.*

The activation energy is extracted by assuming the following simple relation between the scan rate (S_R, which we take as an effective rate imposed on the system) and the temperature:

$$S_R = Ae^{\frac{-E_A}{kT}}$$

Where A is an arbitrary constant, irrelevant for our analysis. Thus, in order to extract the activation energy, E_A, a dataset of scan rates vs. the corresponding temperatures is needed. Since the slow process in both the n-i-p and p-i-n case is ion diffusion across the interfaces, the activation energy in both cases describes essentially the same process, with the difference being the contact material to the perovskite layer. Therefore if as an example, all the data points that yield HF=X, where X can be a minimum, intermediate or maximum HF value are taken, a series of (S_R, T) that will yield the same HF=X value at every point ("iso-HF" dataset) in needed. That is why X is allowed to change between the p-i-n case to the n-i-p case, and the experimentally accessible HF values in our experiments limit us to choose X = minimum HF for the p-i-n case and X = maximum HF for the n-i-p case.

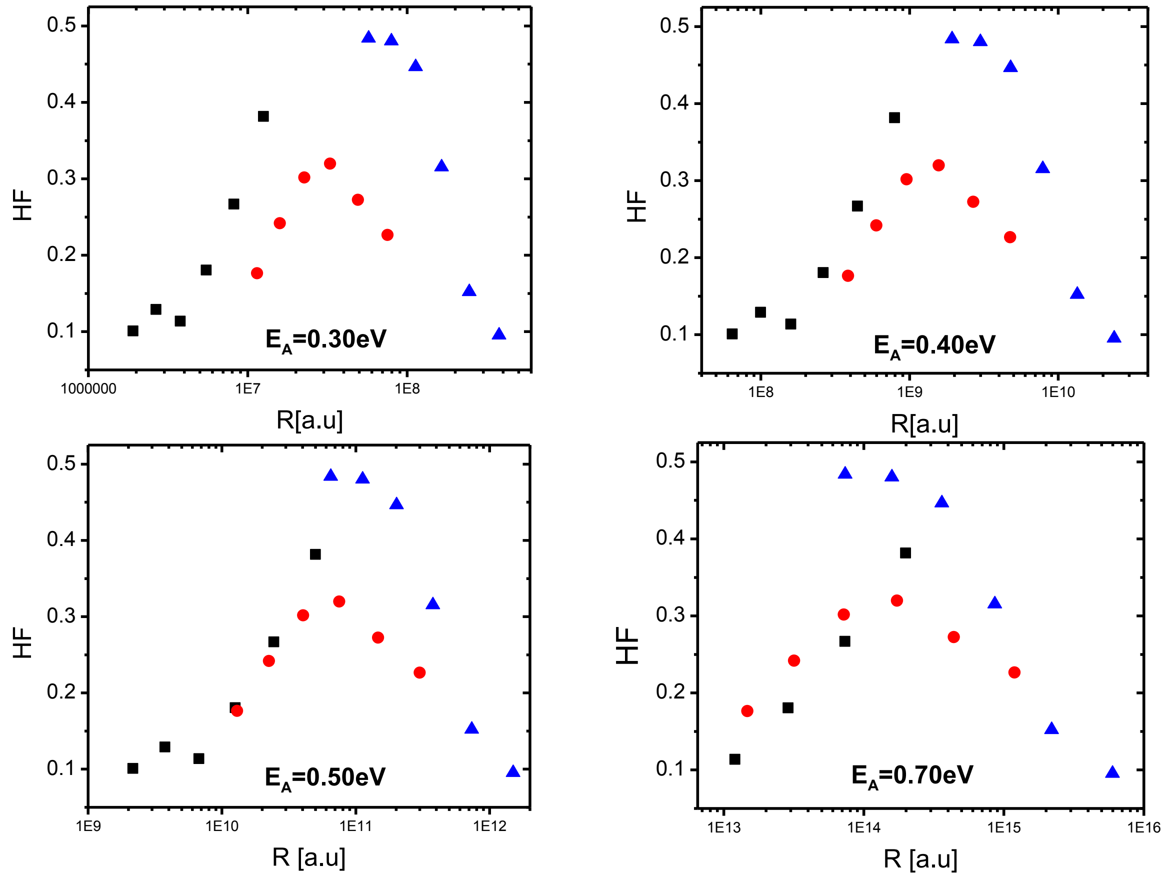

Fig. S10: HF as a function R using different E_A values for the n-i-p device

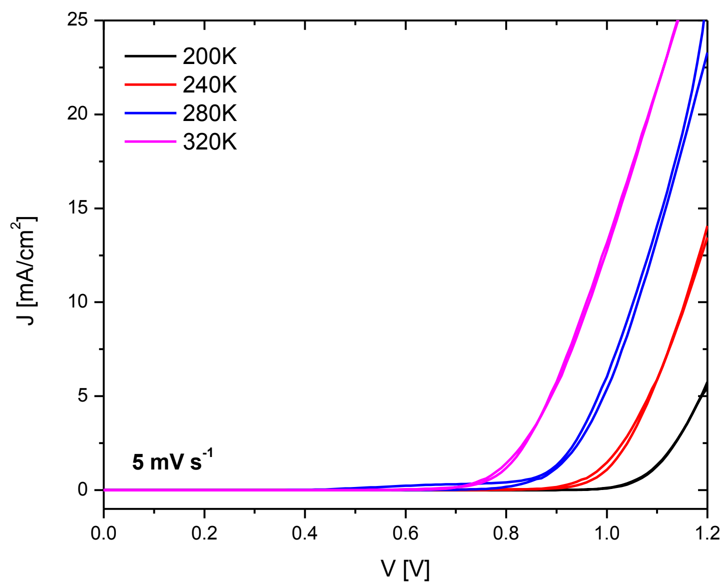

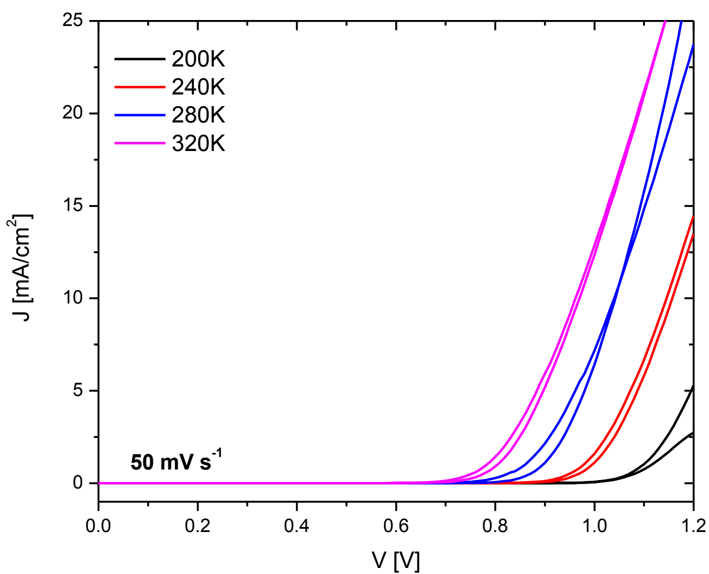

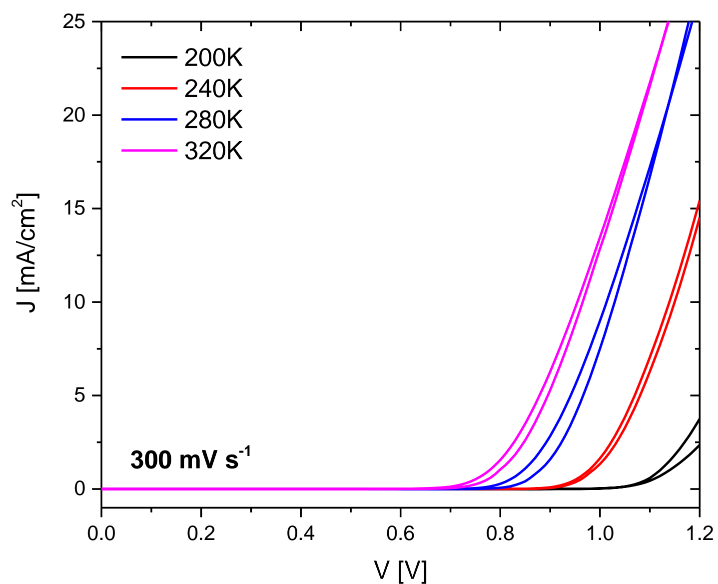

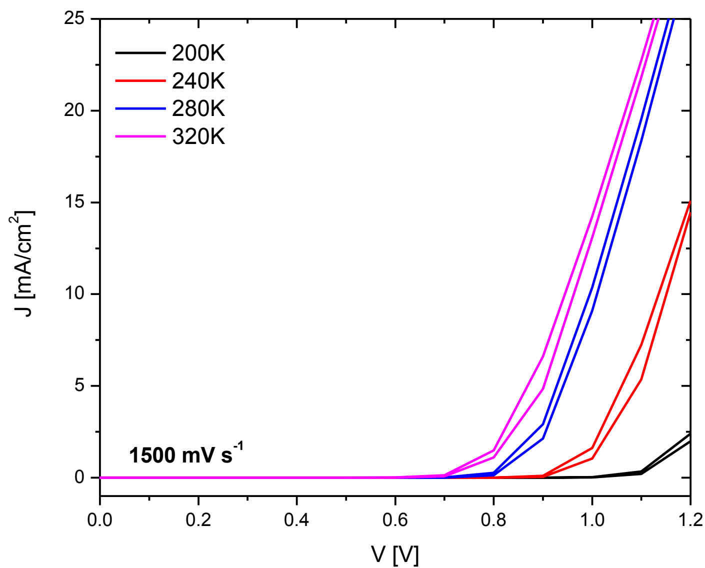

Fig. S11: Dark J-V curves for the p-i-n device as a function of temperature, measured with different scan rates

To calculate the hysteresis factor for the dark curves, a similar definition as shown in Equation (1) was used:

$$HF_{Dark} \equiv \left|1 - \frac{A_{V=0\to V=1.2V}}{A_{V=1.2V\to V=0}}\right| \quad \text{(S1)}$$

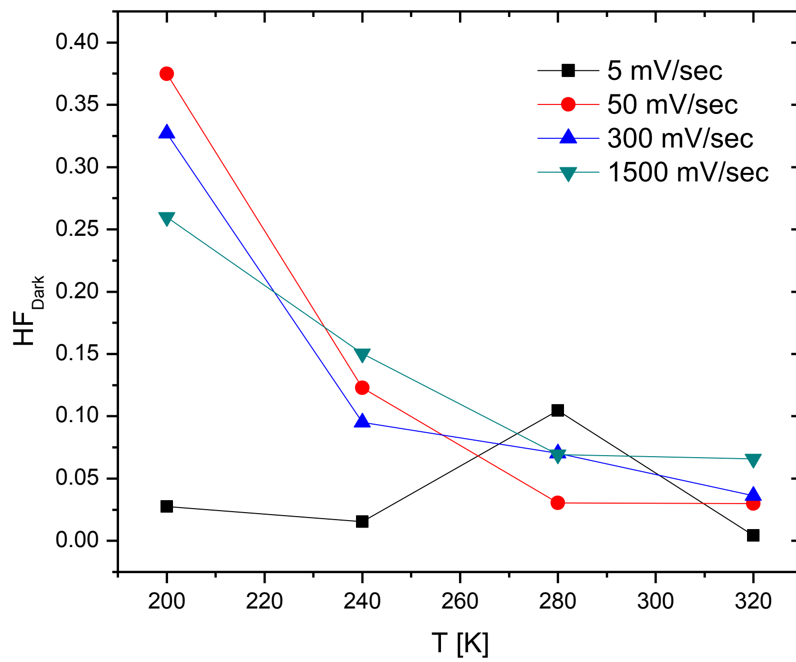

Fig. S12: Hysteresis factor for the p-i-n device in the dark as a function of temperature, for different scan rates

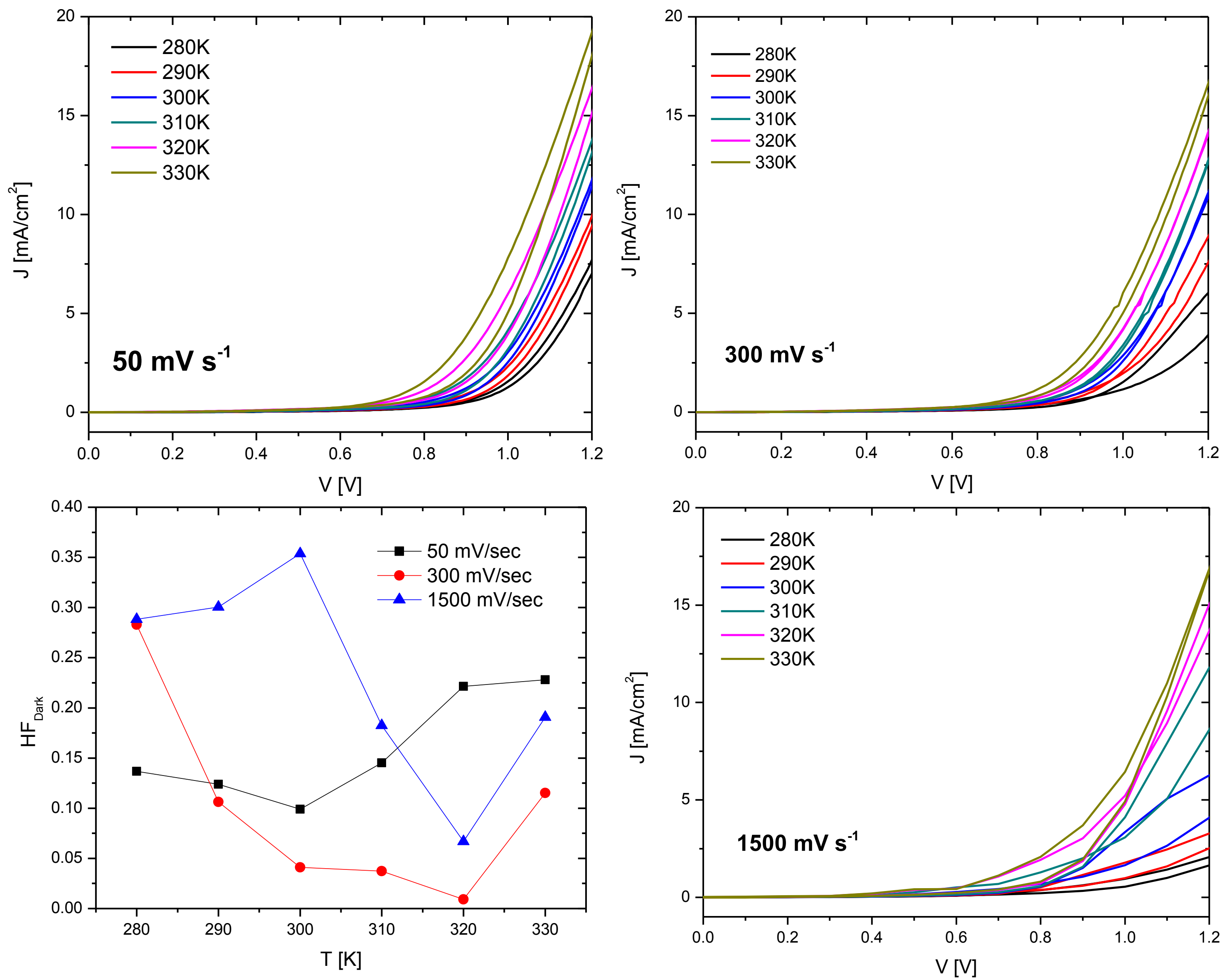

Fig. S13: Dark J-V curves (top; bottom left) and hysteresis factor (bottom right) for the n-i-p device as a function of temperature and for different scan rates: 50mV s^{-1} (top left); 300mV s^{-1} (top right); 1500mV s^{-1} (bottom left).

Modelling traps in perovskite solar cells

A. The numerical model to describe perovskite solar cell operation

To model the device operation of perovskite solar cells a numerical model is used which describes carrier injection, transport, generation, recombination, and trapping for electronic and ionic charges.[1-4] This model solves the Boltzmann transport equations and Poisson's equation on a 2D grid by forward integration in time. In the next paragraphs a detailed description is given on the methods to describe charge transport, carrier injection and carrier recombination. Additional optional processes like i) charge trapping and ii) trap-assisted recombination are included in the numerical model as well. Parameters that need to be defined for each calculation are shown in Table A1. Here CB and CV are the conduction band and valence band, respectively.

TABLE A1. Input parameters for the numerical model of a perovskite solar cell.

Parameter	Symbol
Mobility (electron; hole; anion; cation)	μ_n ; μ_p ; μ_a ; μ_c
CB and CV of semiconductors	E_{HOMO} ; E_{LUMO}
Density of states of semiconductors	N_0
Anion and cation density	a ; c
Work function of contacts	φ
Bias voltage	V_{bias}
Temperature	T
Relative dielectric constant	ε_r

A.1 Charge transport

In the 2D model a rectangular grid is used with grid points at the corners of each cell. The areas of the cells are determined by the widths of the columns and rows which can be specified per row or column. For each cell a material type is specified, either gate, contact, dielectric or semiconductor. Calculations of current, recombination, etc. are performed on the grid points. The 4 cells surrounding the grid point are in equilibrium with each other, which is effectuated by area-average weighting of these 4 cells. Consequently, a single quasi Fermi level is defined on each grid point.

Carrier transport is described by the following Boltzmann transport equations:

$$J_i = -q\mu_i n_i \nabla\psi_{F,i}, \quad \textbf{(S1)}$$

where q is the elementary charge, μ_i and n_i are the mobility and density for free electrons ($n_i = n$), free holes ($n_i = p$), free anions ($n_i = a$), or free cations ($n_i = c$) and $\psi_{F,i}$ is the quasi Fermi energy which is given by

$$\psi_{F,n} = \psi_L - \frac{kT}{q}\ln\frac{n}{N_0}, \quad \textbf{(S2)}$$

$$\psi_{F,p} = \psi_H + \frac{kT}{q}\ln\frac{p}{N_0}, \quad \textbf{(S3)}$$

$$\psi_{F,a} = V - \frac{kT}{q}\ln\frac{a}{N_0}, \quad \text{(S4)}$$

$$\psi_{F,c} = V + \frac{kT}{q}\ln\frac{c}{N_0}, \quad \text{(S5)}$$

where $\psi_L = E_{CB} + V$and $\psi_H = E_{VB} + V$ and V is the electrostatic potential. k is Boltzmann's constant and T is the temperature. Einstein's relation between the diffusion constant and the mobility is assumed to hold. The ion current is zero at the electrodes, for the electrodes are ionically blocking. The continuity equations are

$$\frac{dn}{dt} = \frac{1}{q}\frac{dJ_n}{dx} - R, \quad \text{(S6)}$$

$$\frac{dp}{dt} = -\frac{1}{q}\frac{dJ_p}{dx} - R, \quad \text{(S7)}$$

$$\frac{da}{dt} = \frac{1}{q}\frac{dJ_a}{dx}, \quad \text{(S8)}$$

$$\frac{dc}{dt} = -\frac{1}{q}\frac{dJ_c}{dx}, \quad \text{(S9)}$$

for electrons, holes, anions, and cations, respectively. Here J_i is the current density of particle i and R is the recombination rate. The potential profile throughout the device is calculated from Poisson's equation:

$$\nabla^2 V = -\frac{q}{\varepsilon_0 \varepsilon_r}(p - n + c - a), \quad \text{(S10)}$$

where ε_0 and ε_r are the dielectric and the relative dielectric constant, respectively.

A.2 Carrier injection

To describe the injection of electrons and holes into the semiconductors, the following parameters are of importance: the VB and CB levels of the semiconductor; the Fermi level of the contacts; and the charge carrier density in the semiconductor at the interface. The injection model is based on Boltzmann injection:

$$n(1) = N_0 \exp\left(-\frac{q\varphi_n}{kT}\right), \quad \text{(S11)}$$

where $n(1)$ is the electron density at the first grid-point next to the electrode and φ_n is the injection barrier height. In this model injection is not affected by the grid-point spacing.

A.3 Charge trapping

The charge trapping rate for electrons (T_n) is described by the product of the free electron density (n), the available trap density (N_t-n_t), and a trapping coefficient (in m^3s^{-1}):

$$T_n = c_n \cdot (N_t - n_t) \cdot n. \quad \textbf{(S12)}$$

Detrapping of electrons (D_n) is described by:

$$D_n = c_n \cdot N_0 \cdot n_t \cdot exp\left(-\frac{E_t}{kT}\right), \quad \textbf{(S13)}$$

where N_0 is the density of states and E_t is the trap energy. Empty traps are considered neutral.

A.4 Recombination

Recombination of free electrons and free holes can be described by a Langevin process, including a (Langevin) prefactor as described in ref [5]:

$$R_f = L_{pre} \frac{q(\mu_n + \mu_p)}{\varepsilon_0 \varepsilon_r} \cdot p \cdot n, \quad \textbf{(S14)}$$

where R_f is the recombination rate of free carriers and L_{pre} is the prefactor.[5]

Recombination between trapped electrons and free holes is also described by a Langevin process in the model:

$$R_t = L_{pre,t} \frac{q(\mu_p)}{\varepsilon_0 \varepsilon_r} \cdot p \cdot n_t = c_n \cdot p \cdot n_t, \quad \textbf{(S15)}$$

where R_t is the recombination rate of free holes and trapped electrons, n_t is the trapped electron density, c_n is the recombination coefficient for this recombination process, and $L_{pre,t}$ the Langevin prefactor for this specific recombination process.

A.5 Used parameters

Here follow the parameters we used to model a perovskite solar cell. A grid was used with 4 nm grid-point spacing (see Fig. A1). Model parameters for the electron transport material (ETM), the perovskite, and the hole transport material (HTM) are shown in Table A2 and are based on TiO_2[6] and Spiro-OMeTAD, respectively. For the perovskite, an equal electron (μ_n) and hole (μ_p) mobility was chosen similar to literature values.[7,8] The dielectric constant ε_r was set at 6.5.[9] A weakened form of Langevin recombination was assumed by addition of a prefactor L_{pre} = 10^{-5} in the recombination rate equation.[5] Homogeneous generation G of free electrons and holes was assumed throughout the perovskite layer 2.5 $nm^{-3}s^{-1}$ to model light conditions roughly equal to 1 sun.[10] Doping in the transport layers was modelled by a homogeneous density of immobile anions (a) or cations (c) which are electrostatically compensated by mobile electrons (n) and holes (p).

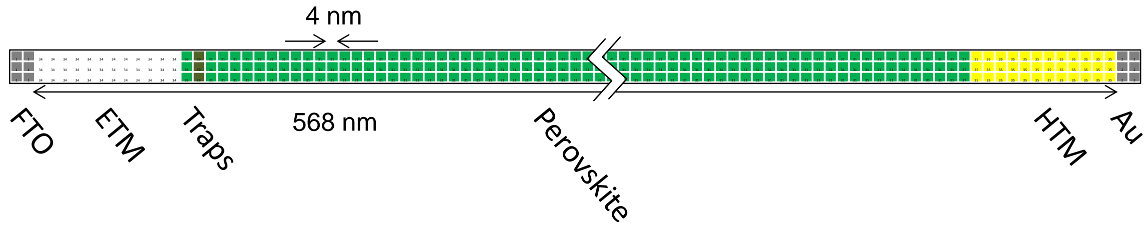

FIG. A1. Grid layout of the modelled perovskite solar cell.

The energy level diagram is shown in Fig. A2.

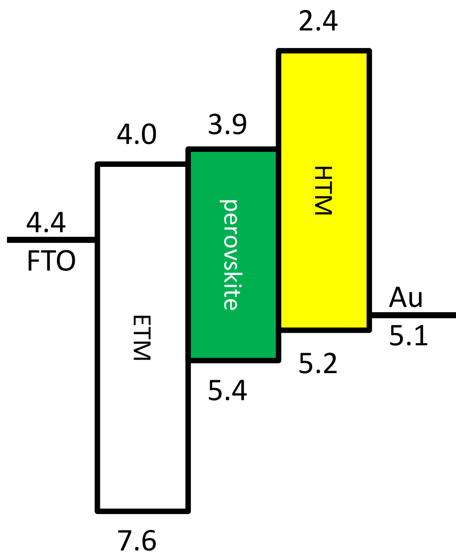

FIG. A2. Energy level diagram in eV of the simulated perovskite solar cell.

TABLE A2. General device model parameters.

property	unit	ETM	Perovskite	HTM
μ_p, μ_n	$cm^2 V^{-1} s^{-1}$	0.02	2	0.02
ε_r	-	80	6.5	3
L_{pre}	-	1	10^{-5}	1
G	$cm^{-3} s^{-1}$	0	$2.5{\cdot}10^{21}$	0
initial a	cm^{-3}	0	X	$1{\cdot}10^{17}$
initial c	cm^{-3}	$4{\cdot}10^{17}$	X	0
Initial n	cm^{-3}	$4{\cdot}10^{17}$	0	0
initial p	cm^{-3}	0	0	$1{\cdot}10^{17}$
Layer thickness	nm	48	472	48
N_0	cm^{-3}	10^{20}	10^{20}	10^{20}

Trapping of electrons at the interface was described by equation S12. The trap energy was set at 0.2 eV at the n-type interface (see Fig. A1.). The trap density was set at 10^{17} cm^{-3}. The trapping coefficient c_n

was approximated by the product of the site volume (i.e. $nDOS^{-1} = 1/2.2{\cdot}10^{24} = 5{\cdot}10^{-25}$ m^3 following [7]) and the attempt frequency which can be related to the phonon frequency, which is typically 10^{-10} – 10^{-12} s^{-1}. Hence c_n was set at $6x10^{-13}$ m^3s^{-1} for interface traps.

The dielectric constant used for the perovskite layer was 6.5, previously it was found [11] that a dielectric constant of 30 does not change the results qualitatively, the change is quantitative (~10% weaker hysteresis), but qualitatively the result is the same (the same trends and behavior can be observed).

Recombination between trapped electrons and free holes in the bulk perovskite was described by equation S14 where $L_{pre,t}$ was maintained at 10^{-5},[5] similar to recombination between free electrons and holes in the perovskite.

A.6 Model operation

Initially no electrons or holes are present. Only at the electrodes electrons and holes are present due to the boundary conditions imposed by the injection model. In addition, the bias voltage is applied to one of the contacts (Au), whereas the other contact (FTO) is set at 0 V. For a defined number and size of time steps, the model then calculates the Fermi energy of all the carriers, solves the Boltzmann transport equations, accounts for electron-hole recombination, and solves the continuity equations to determine the new carrier densities at each grid point. A steady-state solution is obtained when the current, which is determined by the sum of current through the contacts, becomes constant.

References:

1 S. van Reenen, P. Matyba, A. Dzwilewski, R. A. J. Janssen, A. Edman, and M. Kemerink, *Adv. Funct. Mater*. **21**, 1795 (2011).

2 S. van Reenen, P. Matyba, A. Dzwilewski, R. A. J. Janssen, L. Edman, and M. Kemerink, *J. Am. Chem. Soc.* **132**, 13776 (2010).

3 S. van Reenen, R. A. J. Janssen, and M. Kemerink, *Org. Electron.* **12**, 1746 (2011).

4 S. B. Meier, S. Van Reenen, B. Lefevre, D. Hartmann, H. J. Bolink, A. Winnacker, W. Sarfert, and M. Kemerink, *Adv. Funct. Mater*. **23**, 3531 (2013).

5 C. Wehrenfennig, G. E. Eperon, M. B. Johnston, H. J. Snaith, and L. M. Herz, Adv. Mater. **26**, 1584 (2014).

6 E. L. Ratcliff, J. Meyer, K. X. Steirer, N. R. Armstrong, D. Olson, and A. Kahn, *Org. Electron*. **13**, 744 (2012).

7 T. Minemoto and M. Murata, *J. Appl. Phys.* **116**, 054505 (2014).

8 S. D. Stranks, G. E. Eperon, G. Grancini, C. Menelaou, M. J. P. Alcocer, T. Leijtens, L. M. Herz, A. Petrozza, and H. J. Snaith, *Science* **342**, 341 (2013).

9 M. Hirasawa, T. Ishihara, and T. Goto, *J. Phys. Soc. Jpn*. **63**, 3870 (1994).

10 J. M. Foster, H. J. Snaith, T. Leijtens, and G. Richardson, *SIAM J Appl Math* **74**, 1935 (2014).

11 S. van Reenen, M. Kemerink, and H. J. Snaith, *J. Phys. Chem. Lett.* **6**, 3808 (2015).